Changes of the cosmic-ray mass composition in the 10^{14}–10^{16} eV energy range

K. Bernlöhr, W. Hofmann, G. Leffers, V. Matheis,
M. Panter, R. Zink

Max-Planck-Institut für Kernphysik,
Postfach 103980, 69029 Heidelberg, Germany

December 16, 1997

Abstract

Data taken with ten Cosmic Ray Tracking (CRT) detectors and the HEGRA air-shower array on La Palma, Canary Islands, have been analysed to investigate changes of the cosmic-ray mass composition at the 'knee' of the cosmic-ray flux spectrum near 10^{15} eV energy. The analysis is based on the angular distributions of particles in air showers. HEGRA data provided the shower size, direction, and core position and CRT data the particle track information. It is shown that the angular distribution of muons in air showers is sensitive to the composition over a wide range of shower sizes and, thus, primary cosmic-ray energies with little systematic uncertainties. Results can be easily expressed in terms of $\langle \ln A \rangle$ of primary cosmic rays. In the lower part of the energy range covered, we have considerable overlap with direct composition measurements by the JACEE collaboration and find compatible results in the observed rise of $\langle \ln A \rangle$. Above about 10^{15} eV energy we find no or at most a slow further rise of $\langle \ln A \rangle$. Simple cosmic-ray composition models are presented which are fully consistent with our results as well as the JACEE flux and composition measurements and the flux measurements of the Tibet ASγ collaboration. Minimal three-parameter composition models defined by the same power-law slope of all elements below the knee and a common change in slope at a fixed rigidity are inconsistent with these data.

1 Introduction

Cosmic rays from outside the solar system show a smooth flux spectrum and are almost entirely made up of protons and fully ionized nuclei. Except for spallation products, the fluxes of all nuclei follow essentially the same $E^{-2.7}$ power-law in the GeV to TeV energy range, where the primaries can be identified by direct measurements in space- or balloon-borne experiments. Only at higher energies the overall cosmic-ray flux spectrum shows two distinct features near 10^{15} and $10^{18.5}$ eV, as determined by indirect ground-based experiments. Near 10^{15} eV (the *knee*) the spectrums steepens to about $E^{-3.0}$ and seems to become flatter again between 10^{18} and 10^{19} eV (the *ankle*).

Despite lack of direct evidence, there is general consensus that the majority of cosmic rays in the energy range up to the knee should be accelerated at the shock waves of supernova remnants (SNR). For reviews of shock acceleration see [1] and [2]. Cosmic rays diffuse out of the Galaxy on a timescale of 10^7 years and less. SNR can easily provide enough power to refurbish the cosmic rays. Stochastic shock acceleration models and a transformation of source spectra due to an energy-dependent diffusion coefficient can explain the observed power-law spectrum up to 10^{14} eV or perhaps even 10^{15} eV. In contrast, there are no generally accepted source models for the ultra-high energy (UHE) cosmic rays above 10^{15} eV. Unfortunately, the cosmic-ray flux at the knee and higher energies is too small for direct composition measurements. Therefore, little is known about the composition in the UHE range. Several results from ground-based air-shower experiments indicate that the average mass rises near the knee but also evidence for little change or even the opposite effect has been presented (for recent reviews see for example [3, 4, 5]).

In recent years, several large air-shower experiments have been supplemented by additional detector types which enable them to measure composition-sensitive quantities on a statistical basis (not on an event-by-event basis) and compare these to expected values from shower simulations. In general the methods are based on different ratios of the numbers of muons to the numbers of electrons or on the different longitudinal development of showers initiated by different primaries. For such methods both the accuracy of the shower simulations and of the understanding of detector effects (and how well they can be included in the simulations) is important. This also applies to experiments attempting an identification of primaries on an event-by-event basis.

Results presented in this paper are based on a statistical method making use of the angular distributions of particles in air showers. The method has been described in detail in [6]. Its major advantages are small systematic errors because detector effects are understood very well and because shower simulations with different interaction codes give very similar results. There is also sufficient overlap in energy with direct measurements to check for any systematic errors.

The analysis is mainly based on the angular projections of shower particles in a reference frame defined by the positions of the respective tracking detector and the shower core position. The *radial plane* is defined here as a vertical plane passing through detector and core positions, and the *tangential plane* as a vertical plane perpendicular to the radial plane. The *radial (tangential) angle* is the angle between the shower and the track projected onto the radial (tangential) plane (see figure 1). Except for vertical showers, the shower axis is, in general, not exactly in the radial and tangential planes. Since the analysis was restricted to showers with zenith angles of less than 30 degrees, this definition is essentially equivalent

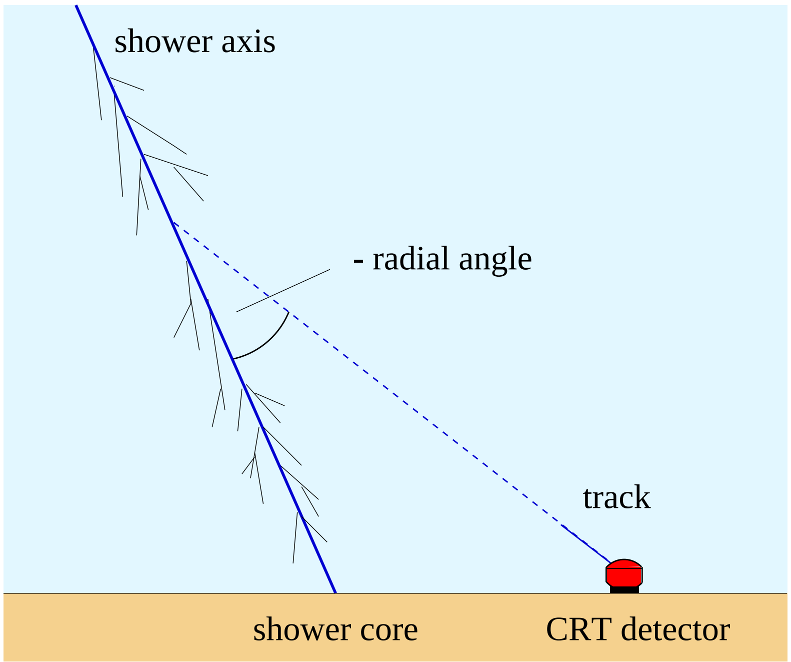

Figure 1: Radial angles are defined as the angles between shower axis and particle track in the projection into a vertical plane through the core and the CRT detector location. Note that particle coming from the shower axis have, in the definition of this work, a negative radial angle.

to one where radial and tangential planes are parallel to the shower axis instead of to the vertical (see [6]).

The measured average radial angles are closely related to the average longitudinal shower development, with earlier development (heavier nuclei) corresponding to radial angles closer to zero. Most muons are produced near the shower axis and are rarely deflected by more than a few tenths of a degree due to multiple scattering and the geomagnetic field. Thus, muon radial angles can, in principle, be transformed into muon production heights for any given core distance. Since statistical and systematic errors are much easier to understand directly in terms of measured angles, no such transformation is used here. Radial angle distributions are used as a measure of the average longitudinal shower development while tangential angles give a measure of our angular resolution (since the experimental resolution substantially exceeds the intrinsic scatter).

2 Experimental setup and data handling

The Cosmic Ray Tracking (CRT) project had the initial goal to build a large air-shower array with tracking detectors [7]. Compared to scintillator arrays, such an array of tracking devices would promise a lower threshold energy [8] and good angular resolution even for small shower sizes. To search for gamma-ray sources, a substantial reduction of the hadronic background by a very clean muon identification was one of the design goals.

The detectors which emerged out of the CRT project consist of two 2.5 m^2 circular drift chambers of the TPC (time projection chamber) type on top of each other, and a 10 cm thick iron plate as a muon filter between both chambers [9]. Each chamber has six readout wires with charge-division and segmented cathode strips for fully three-dimensional track reconstruction in each chamber. The whole detector is in a gas-tight container filled with an argon-methane gas mixture.

Readout is performed through a 40 MHz FADC system into a local computer system next to each CRT detector. Tasks performed by these computers include detector control and monitoring but also online track reconstruction and calibration. Ten prototype detectors were installed and operated at the site of the HEGRA air-shower experiment [10, 11] at the Roque de los Muchachos Observatory on La Palma, Canary Islands for about three years (1993–1996). The primary goal of this installation was to test this new type of cosmic-ray detectors which met all anticipated design goals. These goals included an angular resolution of 0.4°, a muon-electron discrimination better than 10^{-3}, and robustness at mountain altitude conditions [12]. In conjunction with the HEGRA array, the investigation of the cosmic-ray mass composition has been the major scientific application of this installation.

The HEGRA experiment [10, 11] is a multi-component air-shower installation with a detector array and an independent Cherenkov telescope system. During the time when the data presented here were taken, the detector array consisted of 221 scintillator stations of 1 m^2 area each (see figure 2), 49 open photomultipliers with light cones measuring Cherenkov light (AIROBICC), and 17 detectors of 16 m^2 area each with six layers of Geiger tubes. Array data covering part of the time when CRT detectors were operated with array trigger have been kindly provided by the HEGRA collaboration. For the independent HEGRA analysis methods and results see [11] and references therein. For the analysis presented here, only data from the scintillator array have been combined with the CRT data. Data from the other HEGRA array components have not been used because these components were in operation only during a small part of the time when the CRT detectors were operated with HEGRA triggers and there are not enough combined data available at energies above about 10^{15} eV.

For some of the detector tests and for the composition studies, the array of CRT detectors was triggered by the HEGRA array and event numbers were synchronized by the central CRT electronics system. For the detector tests it was desirable to have many CRT detectors in a rather small area while for the composition studies a better configuration has detectors distributed over a larger area. As a compromise, two CRT detectors were installed outside of the HEGRA array on two existing helicopter ports (see figure 2). With this configuration it was possible to measure shower particles at core distances up to 300 m. For about half of the time covered in the analysis all ten CRT detectors were triggered by HEGRA. During the rest of the time the eight detectors inside the HEGRA array were op-

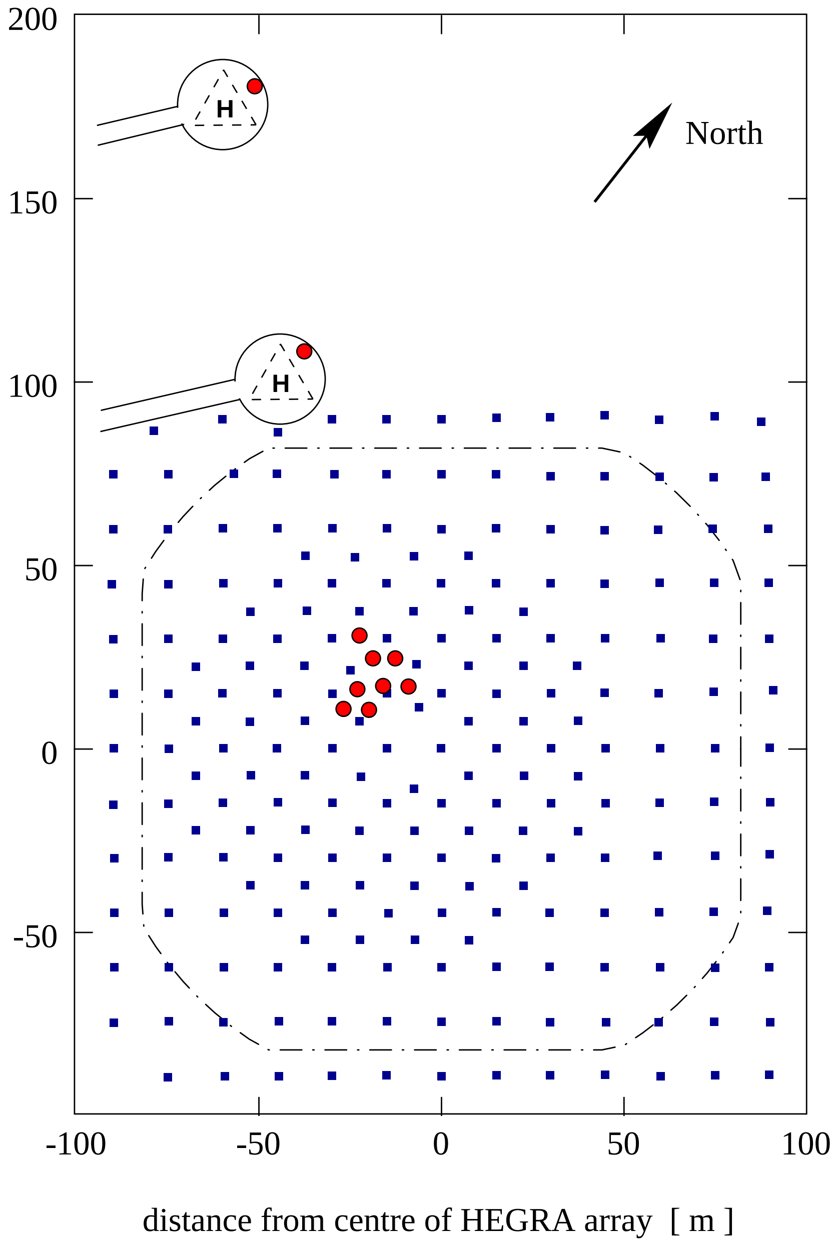

Figure 2: Map of the HEGRA site showing only the scintillator stations (square dots) and CRTs (circles). The dash-dotted line marks the area of shower core positions accepted in the analysis.

erated independently of HEGRA for detector tests while the two on the helicopter ports were taking data with HEGRA triggers.

The HEGRA and CRT arrays were only loosely coupled, i.e. triggers, run and event numbers, and Rubidium clock information was exchanged but data were recorded separately. Initially, the CRT detectors recorded partially processed hit data (pulse areas and drift times). The track reconstruction and calibration for these data were done offline. After the relevant algorithms had been checked [12] the complete reconstruction and calibration was done online by the computers at the CRT detectors. For the HEGRA scintillator array, the ADC and TDC data for all triggered stations were recorded. Shower reconstruction, i.e. reconstruction of the arrival direction, the position of the shower core, and the shower size, was done offline. HEGRA data were made available after this data reduction and merged with the corresponding CRT data. The available amount of data for this analysis corresponds to a total life time of 42 days, scattered over a period of about one and a half years.

3 Simulations

In extensive air showers where particles are observed after several interaction lengths of the particle cascade, any quantitative interpretation of data requires comparison with simulations of physical processes in the showers as well as in the detectors. Shower simulations are based on the CORSIKA [13] program in versions 4.068 and 4.50. Simulations with different interaction models were used to obtain an estimate of systematic errors due to differences in interaction models. As the more sophisticated and, therefore, presumably more accurate model we used the CORSIKA option with VENUS [14] above 80 GeV energy and GHEISHA [15] at lower energies. Completely different interaction models are provided by the DPM (dual parton model inspired) and the Isobar interaction models above and below 80 GeV, respectively. For some of the simulations, the showers were fully simulated, including the electromagnetic subshowers. All simulations were done for the HEGRA site on La Palma.

As far as the comparison with muon angular distributions are concerned, it turned out that for showers well above the HEGRA trigger threshold it is sufficient to take the shower sizes from the summed analytical estimates of the electromagnetic subshowers. Without full simulation of the electromagnetic part a much larger number of showers could be simulated without exceeding manageable amounts of disk and tape storage. In total about 30000 proton and about 15000 iron showers have been simulated, most of them in the energy range from 20 TeV to 10 PeV for protons and from 40 TeV to 20 PeV for iron. Some simulations extend down to lower energies. The zenith angles of simulated showers extend up to 32°.

Simulations have also been done for showers initiated by helium, nitrogen (representing the CNO group), and magnesium nuclei (representing Ne to S) in order to evaluate realistic mixed compositions like those measured by JACEE up to a few hundred TeV [16, 17]. All simulations were done with an $E^{-1.7}$ differential flux spectrum and appropriate event weights (e.g. $\propto E^{-1}$) were applied to match a desired flux spectrum.

Shower simulations are followed by simulations of tracking detectors and the array. The simulation of the tracking detectors is quite detailed in the case of muons where multiple scattering and energy loss in the iron plate and their consequences on the detection efficiency and the reconstructed track angles are fully taken into account. Other efficiencies, like those of the identification of electrons, gammas, protons, or pions as either electron tracks (in the upper drift chamber only) or muons (pairs of isolated tracks in both chambers matching in angle to better than 2.5° in both projections) and the relevant angular resolutions were parametrized on the basis of detailed detector simulations with the GEANT [18] package.

The array simulation used is relatively simple and, thus, applied only at shower sizes where HEGRA is fully efficient for showers with cores inside the array. Detailed simulations show that this is the case for shower sizes N_e above 15000. For sizes between 10000 and 15000 HEGRA should be already 95% efficient.

Because the HEGRA scintillation counters are covered by 5 mm of lead, the measured shower sizes N_h do not represent the numbers of charged particles above the lead but below. A fit to Monte Carlo simulations [19] shows that, on average, a relation

$$N_\mathrm{h}/N_\mathrm{e} = (1.7 \pm 0.2)\,(N_\mathrm{e}/10000)^{-0.14\pm0.04} \tag{1}$$

holds at least in the range $5 \times 10^3 < N_h < 10^6$. This is independently confirmed by comparing the experimental relation between the number of fired scintillation counters and the reconstructed N_h with the simulated relation between the number of scintillation counters and the N_e number given by CORSIKA. The statistical accuracy of N_h reconstruction is also obtained from simulations [20] and is included as an additional source of shower size fluctuations.

The angular resolution and the accuracy of the core location are parametrized as functions of HEGRA shower size and zenith angle. The resolutions of shower size and core location are taken from detailed array simulations [19, 20]. Their roles are relatively uncritical for the analysis presented in the following section. For the array angular resolution see also the next section.

After folding in the HEGRA angular, core, and size resolutions, the same cuts as to measured data were applied and all tracks were filled in histograms of identical bin sizes as with the measured data. Each track was given a weight corresponding to the probability that a particle (muon, electron, proton, pion, etc.) would be identified as a muon times the event weight which corrects from the $E^{-1.7}$ differential spectrum of simulated showers to the assumed actual spectrum with or without a knee.

4 Analysis

The tangential angles of muons have a very narrow intrinsic distribution (see [6]) and are used to derive the combined angular resolution of CRT tracks and HEGRA showers as functions of shower size, zenith angle and core distance. The HEGRA angular resolution assumed in the simulations was chosen such that the measured width of the tangential angle distribution was reproduced in all cases.

The radial angles of muons but also of electrons are related to the longitudinal shower development and are sensitive to the composition. With the 25 m^2 total area of the ten CRT detectors there is rarely more than one muon and only a few electrons recorded in a typical event, and statements on an event-by-event basis are not possible. Therefore, this analysis is based on the *inclusive* radial angle distributions and their comparison with simulations. In particular, we use the median radial angle as a function of core distance in different intervals of the shower size.

The shower parameters, i.e. core position, reconstructed size N_h, and direction are obtained from the HEGRA shower reconstruction [19, 21]. For about 10% of the data both the scintillator array and the AIROBICC array of open Cherenkov counters was operational. For this part of the data, the shower direction is available separately from both arrays. It turned out that median radial angles of muon tracks with respect the AIROBICC shower direction follow the same curve (as a function of core distance) for all CRT detectors. With respect to the scintillator array, shower direction deviations of up to a few tenths of a degree became apparent, in particular for core positions near the edge of the array. This seems to be due to the fact that the particles in the shower are much more concentrated near the shower axis than the Cherenkov light and the scintillator array is thus more sensitive to errors in cable delay calibrations. To correct for that effect after the shower reconstruction, a correction depending on the core position was applied to scintillator array shower directions. The amount of this correction is just the average difference between shower directions from scintillator array and AIROBICC and is slightly different for data from different periods. By applying the correction we could take advantage of the smaller systematic errors of the AIROBICC shower direction but preserve the ten-fold larger statistics of the scintillator data.

Another calibration aspect which has been very carefully checked is that of the alignment of the CRT detectors. Their alignment with respect to the vertical direction was once measured with a large level mounted on top of the detector containers. Tolerances of the drift chambers inside the containers are of the order of 1 mm on a 2 m radius. All containers were measured before assembly. Changes of the alignment were monitored with built-in clinometers with 0.01° resolution and no changes were found over a two-year period. For the detectors inside the HEGRA array independent measurements of the alignment were obtained from the average angles between tracks and showers for shower cores near (e.g. less than 30 m from) each CRT detector. Both calibrations agree with a r.m.s. scatter of 0.12° and mean differences consistent with $0^\circ \pm 0.05^\circ$.

For the two detectors outside of the array the alignment was checked by triggering them with vertical muons. A purpose-built device with two 5 cm diameter scintillators and photomultipliers in a one meter long tube was mounted and vertically aligned on top of the detectors at the experimental site. Good agreement was also found in that case. Errors in the alignment with respect to the HEGRA zenith direction are estimated to be 0.05° for the detectors inside the HEGRA array and 0.10° for the two detectors outside. Calibration of the azimuthal alignment of CRT detectors with respect to HEGRA is based on the fact that the measured distribution of tangential angles has to be symmetric and centered at zero. This calibration is accurate to 0.02°.

5 Results

Figure 3 shows histograms of muon radial angles for different core distance intervals. Because the distributions have long tails towards large negative radial angles (in the definition used throughout this work, see figure 1), their median values have smaller relative statistical errors than their mean values – opposite to a Gaussian where the median is $\sqrt{\pi/2}$ times worse than the mean. For the comparison with simulations, the median values are also more robust against non-Gaussian tails of the assumed HEGRA angular resolution function and the small fraction of non-shower muons. The statistical errors of the measured median values are derived as a given fraction of the r.m.s. deviation of radial angles. The appropriate fraction is taken from simulations given the expected shapes of the distributions. Although the central limit theorem applies to these medians, it should be kept in mind that probability distributions of the medians are not Gaussian for very small numbers of muons (but still better than distributions of the mean). However, this plays only a role in the largest shower size intervals at large core distances.

Resulting measurements of median muon radial angles in 10 m core distance bins and for six different intervals of shower sizes are shown in figure 4. Energies corresponding to these ranges are summarized in table 1. At shower sizes below about 10^5 which overlap with direct measurements we find very good agreement with the corresponding simulations. Note that for large shower sizes the CRT detectors cannot reconstruct muons near the shower core, mainly because the readout electronics is saturated by the signals of many particles [12].

Neglecting non-Gaussian tails of the median angles, a measure of the cosmic-ray mass composition can be obtained from the average position of measured data between proton and iron simulations:

$$\Lambda = \frac{1}{\sum w_i} \sum_i w_i \frac{\langle\alpha_i\rangle - \langle\alpha_{i,\mathrm{p}}\rangle}{\langle\alpha_{i,\mathrm{Fe}}\rangle - \langle\alpha_{i,\mathrm{p}}\rangle}, \tag{2}$$

where $\langle\alpha_i\rangle$ is the measured median muon radial angle in core distance interval i and $\langle\alpha_{i,\mathrm{p}}\rangle$ and $\langle\alpha_{i,\mathrm{Fe}}\rangle$ are from simulation for pure protons and pure iron nuclei, respectively. The weights w_i take the statistical accuracy of measured data into

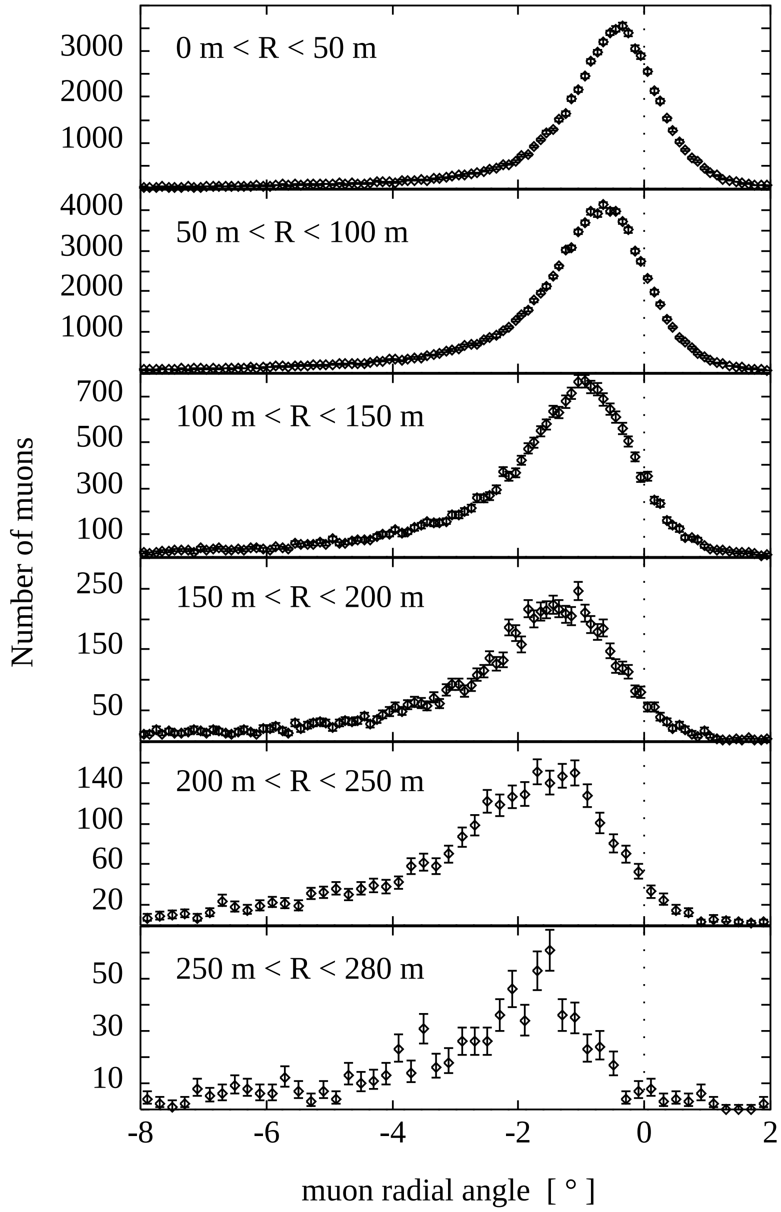

Figure 3: Histograms of muon radial angles in different intervals of core distances for $15000 < N_\mathrm{e} < 50000$ ($24000 < N_\mathrm{h} < 67000$). Note that particles coming from the shower axis have negative radial angles.

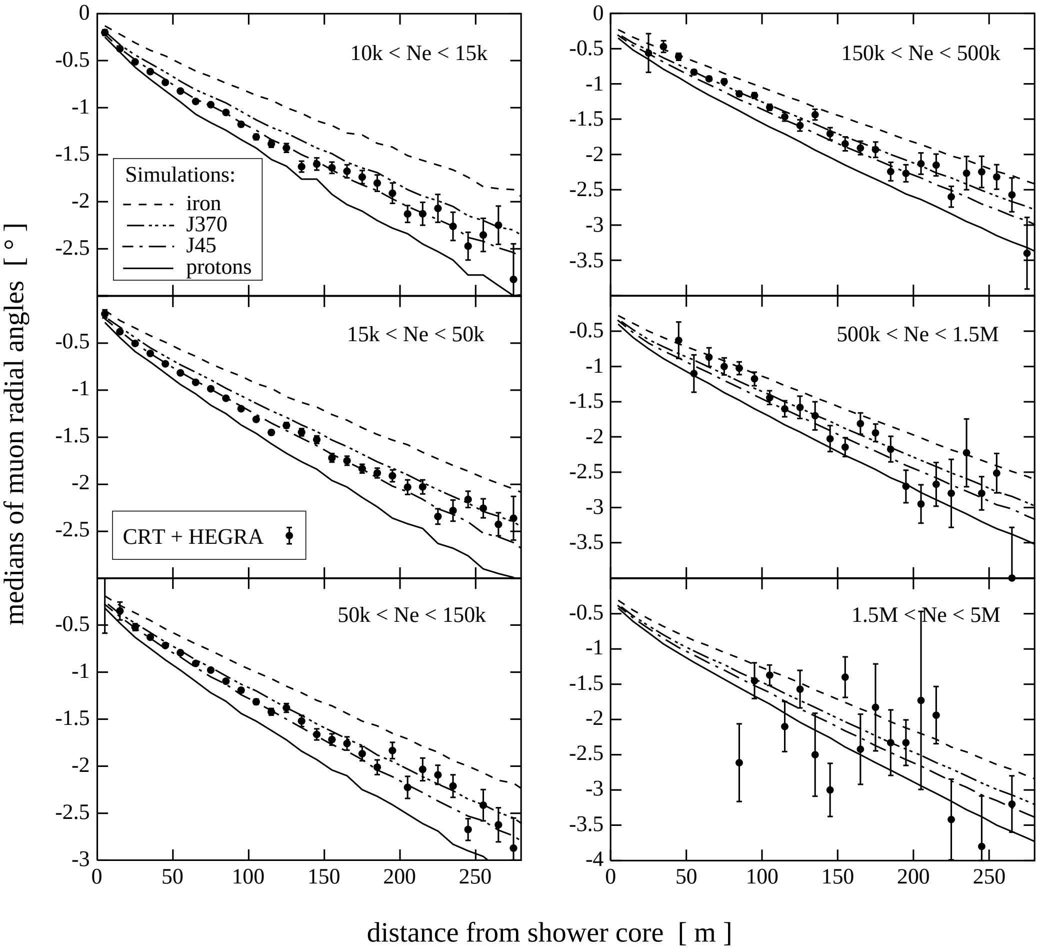

Figure 4: Median radial angles of muons measured with CRT detectors versus the HEGRA shower axis as functions of horizontal distance of the CRT detectors from the shower cores. Simulations are superimposed for pure protons and iron as well as for mixed compositions (assumed energy-independent with an $E^{-2.7}$ spectrum) corresponding to direct measurements of the JACEE collaboration [16] above 45 TeV (J45) and above 370 TeV (J370). Simulations shown are based on CORSIKA interaction options VENUS and GHEISHA.

account. By definition, $\Lambda = 0$ if the data match simulated protons and $\Lambda = 1$ if they match simulated iron.

Least squares fits of Λ times the iron curve plus $(1-\Lambda)$ times the proton curve to the data are equivalent to equation 2. Due to the non-Gaussian tails in case of poor statistics, more appropriate maximum-likelihood (ML) fits with Λ as the only free parameter were actually used. For the ML fits a set of parametrized likelihood functions was obtained from a range of simulated angular distributions like those shown in figure 5. For that purpose, n radial angles ($5 < n < 1000$) were randomly selected many times from the simulations. Histograms of the corresponding median radial angles were stored (one histogram for each core distance interval, each n,

Table 1: Average energies (PeV) of simulated showers in six different shower size intervals, assuming an $E^{-2.7}$ spectrum.

N_e	protons	He	N	Mg	Fe
$(1.0–1.5)\times 10^4$	0.057	0.086	0.12	0.15	0.19
$(1.5–5.0)\times 10^4$	0.105	0.15	0.22	0.25	0.32
$(0.5–1.5)\times 10^5$	0.29	0.41	0.54	0.60	0.78
$(1.5–5.0)\times 10^5$	0.77	1.0	1.3	1.5	1.8
$(0.5–1.5)\times 10^6$	2.3	2.8	3.7	3.9	4.7
$(1.5–5.0)\times 10^6$	5.7	7.2	8.8	9.2	10.5

and each element or element mixture). In a second step a suitable parametrisation was fitted to these histograms and used for the actual ML fits as a third step. The parametrisation takes into account that, for small n, the distributions of medians are, for technical reasons, slightly different for odd and even n. As the statistics improves (n grows), error distributions of the median radial angle values indeed approach a Gaussian and therefore least squares and ML fits become equivalent. Except for the two largest shower size intervals, results from both types of fits in fact differ by less than 0.005 in Λ and its error.

By simulations, the ML fits were checked to have no significant bias for our data even if including core distance bins with only six muons. Such simulations – using one set of simulated angular distributions and the experimentally measured numbers of muons in each distance bin – were also used to verify the experimental statistical errors of our Λ values (see figure 6). That procedure also showed that in the largest shower size interval a least squares fit is less accurate than the applied maximum likelihood fit. Statistical errors of the air-shower simulations were estimated by comparing results obtained with separate subsets of the simulated showers.

It turns out that Λ is a good measure of $\langle \ln A \rangle$, in particular for realistic mixed compositions like those from direct measurements of the JACEE collaboration [16] above 45 TeV and above 370 TeV. In the following, these compositions will be referred to as J45 and J370, respectively. In fact,

$$\Lambda \approx \langle \ln A \rangle \,/\, \ln 56 \qquad (3)$$

holds with good accuracy for mixed compositions (see figure 7), as long as the composition does not change substantially within a factor of 2 in energy and the spectrum slope is near -2.7. For this reason we can define

$$\langle \ln \tilde{A} \rangle = \Lambda \ln 56 \qquad (4)$$

to remind of the above relation ($\langle \ln \tilde{A} \rangle \approx \langle \ln A \rangle$).

There are two notable deviations visible in figure 7. Pure elements between protons and iron are all a bit above the corresponding value of $\ln A \,/\, \ln 56$ but

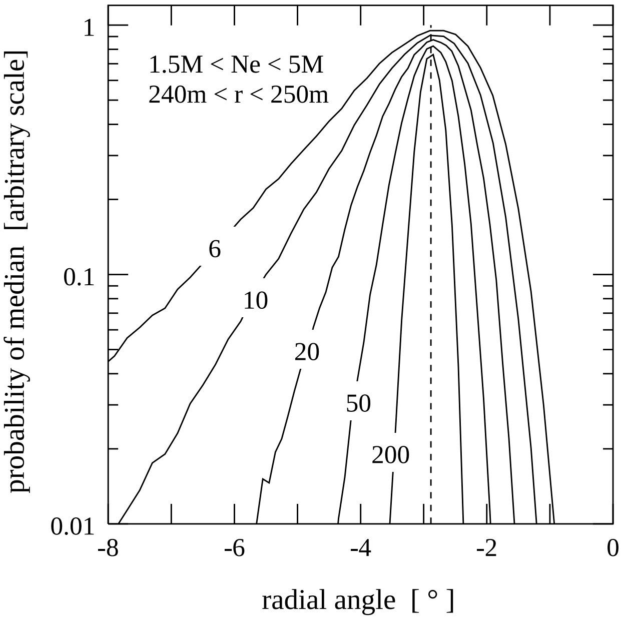

Figure 5: Likelihood distributions (arbitrarily scaled) for median radial angles with 6, 10, 20, 50, and 200 entries in the histogram, based on simulations for one core distance interval (240–250 m) in the largest shower size interval with a J370 composition. Note that the distributions are asymmetric for small numbers of muons but approach a Gaussian with increasing numbers.

slightly falling with shower size as the shower maximum for proton showers is approaching the HEGRA altitude of 2200 m. In the extreme case of a composition made up of only protons and iron, Λ is below $\langle \ln A \rangle \,/\, \ln 56$ for the smaller showers and is rising to the expected value as the difference in energy of proton and iron showers with the same size N_e changes from a factor of 3 to a factor of 2 (see table 1). For realistic mixed compositions both effects cancel remarkably well over the whole range of shower sizes.

For evaluation of experimental Λ values a fixed range of core distances should be preferred where measurements are of good quality over the whole range of shower sizes. Because of the CRT electronics saturation when the detector is hit by more than some 10–20 charged particles (and track reconstruction starting to deteriorate already before that), core distances of less than 80 m were ignored. Note that for the largest size interval we see some saturation up to about 100 m core distance. Punch-through electrons are of no concern for CRT detectors at these large core distances. Occasional non-shower muons are negligible at even the largest core distances and small showers [12]. In the following, results were obtained from data in the 80–280 m core distance range. Reasonable variations of the distance limits (e.g. 100–250 m) give consistent results. Only in the size interval $5 \times 10^5 < N_e < 1.5 \times 10^6$ there was any noticeable dependence on the lower limit of the distance range – which is consistent with a statistical fluctuation but could be an artefact of detector saturation – and this variation has been included

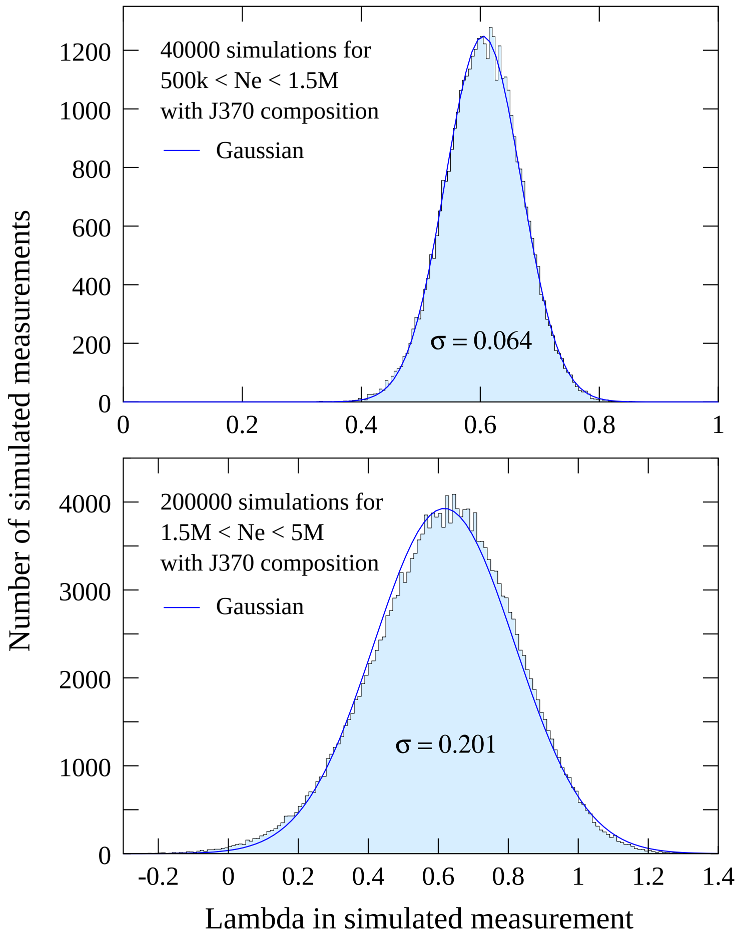

Figure 6: Histograms of resulting Λ values in large numbers of simulated measurements for shower size intervals $5 \times 10^5 < N_e < 1.5 \times 10^6$ (top) and $1.5 \times 10^6 < N_e < 5 \times 10^6$ (bottom). In each core distance interval the same number of muons as in the experimental data was randomly selected from simulations for a J370 composition and the same procedures for calculating medians and the same maximum-likelihood fits were applied as to experimental data. The σ values of the fitted Gaussians correspond to the statistical errors of the measurements.

into the statistical error estimates.

Resulting Λ values for the data from figure 4 depend slightly on the interaction model used for the simulations. Figure 8 and table 2 show results with respect to the VENUS/GHEISHA and the DPM/Isobar model simulations above/below energies of 80 GeV. For both choices of models there is good agreement of our results with direct measurements of JACEE [16, 17], in absolute numbers as well as in the rise of Λ with shower size or energy. Statistical errors for Λ were checked by simulations given the measured numbers of muons in each distance bin.

In addition to the statistical errors shown in figure 8 there are several sources of systematic errors. These are either independent of the shower size, like the calibration of detector alignments (0.06) or only very weakly depending on shower size,

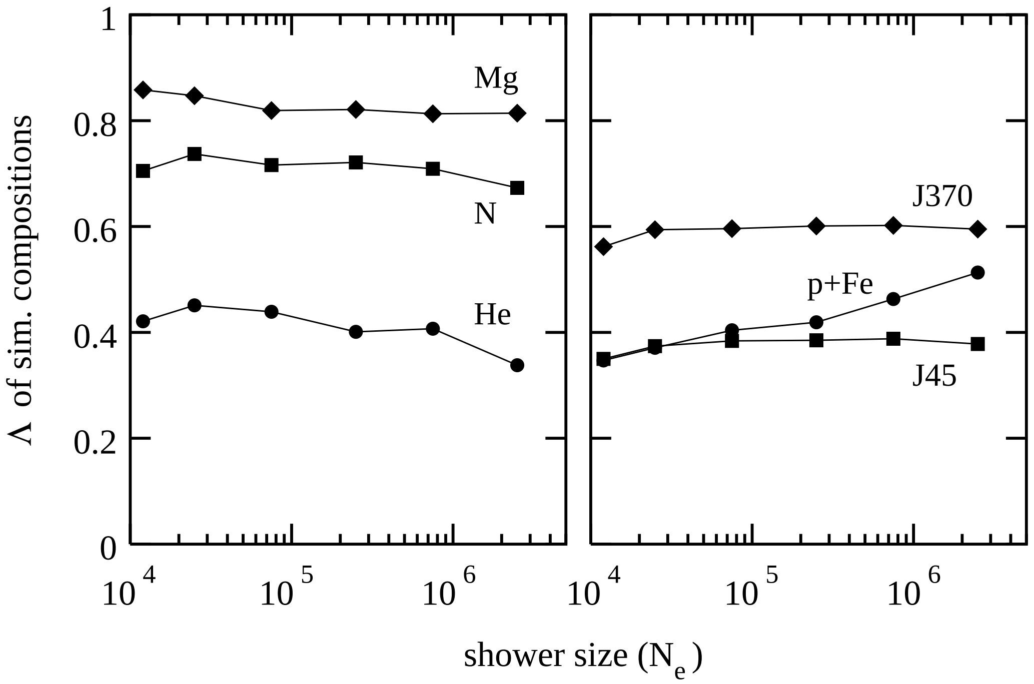

Figure 7: Values of Λ in simulations of pure and mixed compositions (assumed constant with a spectrum slope of -2.7). Left: pure Helium ($\ln A/\ln 56 = 0.344$), Nitrogen (0.656) and Magnesium (0.790). Right: a mixture of 50% protons plus 50% iron ($\langle \ln A \rangle / \ln 56 = 0.5$) and compositions like those measured by JACEE [16] above 45 and 370 TeV ($\langle \ln A \rangle / \ln 56 = 0.379$ and 0.592), respectively.

Table 2: Λ from CRT and HEGRA data as in figure 8.

$\langle N_e \rangle$	Λ with VENUS + GHEISHA	Λ with DPM + Isobar
1.2×10^4	0.35 ± 0.03[1]	0.39 ± 0.03[1]
2.5×10^4	0.43 ± 0.03	0.44 ± 0.03
7.5×10^4	0.50 ± 0.03	0.54 ± 0.03
2.5×10^5	0.57 ± 0.04	0.63 ± 0.04
7.5×10^5	0.57 ± 0.09	0.66 ± 0.09
2.5×10^6	0.55 ± 0.21	0.63 ± 0.19

[1] Statistical errors of data and simulations only. See text for systematic errors.

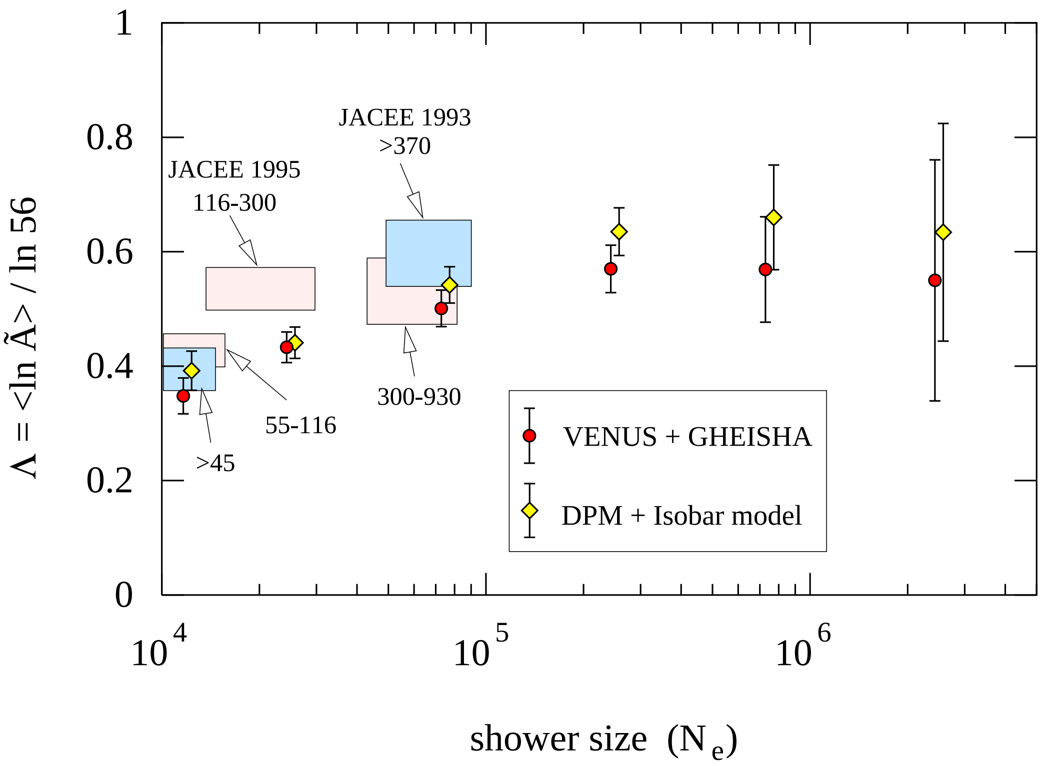

Figure 8: Λ values obtained by comparing CRT/HEGRA data with simulations based on the VENUS/GHEISHA and DPM/Isobar interaction models. Error bars shown include only statistical errors of measured data and simulations. See text for systematic error estimates. For comparison the Λ values corresponding to direct JACEE composition measurements [16, 17] are superimposed at the respective *typical* shower sizes (best matching for helium and medium heavy nuclei, see table 1). The box heights represent quoted statistical errors.

like the relation of shower sizes in equation 1 (0.03 overall plus $0.015\log_{10}(N_e/3\times 10^4)$ size dependent). The systematic error related to the interaction model is estimated as 0.05 (see figure 8) and might depend weakly on shower size. The overall systematic error of Λ is thus estimated as 0.08 (common to all size intervals) and the error of $d\Lambda/d\log_{10}(N_e/3\times 10^4)$ as 0.025. Considering these errors, the agreement with JACEE is remarkably good.

6 Interpretation

Any interpretation of composition measurements should also take the available data on the overall cosmic-ray flux into account. A particularly simple model of the cosmic-ray composition is to assume that there is only one universal type of Galactic cosmic-ray sources and the acceleration time scales as well as the propagation are then only functions of the rigidity $R = pc/Ze$ (p being the momentum). It is well known that such a simple model cannot be matched very well to the older Akeno measurements [22] where the knee appears almost as a single kink in the flux spectrum. The newer Tibet array measurements [23] with a gradual steepening of the spectrum are much closer to expectations for a minimal model but still the steepening of the spectrum has to happen within less than about half a decade of rigidity.

A minimal composition model would be to assume a sudden kink of each component at a given rigidity. Such a simple model is consistent with our composition data alone (for $R_{\mathrm{knee}} \approx 100$ TV, see model 2 in figure 11) or with the flux data of JACEE and the Tibet array [23] alone (for $R_{\mathrm{knee}} \approx 500$ TV, see model 1 in figure 9) but could not be tuned to be consistent with both our composition data and the available flux data. This inconsistency is even more severe if the Akeno flux spectrum [22] is assumed.

Such a simple model is also inconsistent with JACEE composition measurements finding a harder spectrum for the CNO and iron groups of nuclei than for protons and helium near 100 TeV. Although it is usually believed that there is a transition to another dominant source type at the knee, neither are the JACEE data precise enough nor is our measurement of $\langle \ln A \rangle$ sufficient to conclude that such a transition is already seen. If there is a cutoff in the spectrum of one source component (presumably supernova remnants) and a transition to an entirely different one, it is understandable that cutoff and transition should happen at about the same energy but it remains very puzzling that both components should add up to form the knee. Why should the second component not extend with its E^{-3} spectrum to lower energies but just set on at the same energy and with the same flux where the first component cuts off. Assuming there is a transition at the knee, then the second component has a heavier composition but – based on the JACEE data and our $\langle \ln A \rangle$ – not only consisting of iron group nuclei.

Without firm physical models of the cutoff of a first and the onset of a second component there are too many free parameters for reasonable checks. It is perhaps more illustrating to see how an extrapolation of JACEE measurements combined with a rigidity dependent knee compares with composition and flux data. Starting with a composition in the 55–116 TeV energy range and spectral indices of the five groups of nuclei as measured by JACEE [17], there are just two parameters in such models: the rigidity of the knee for each element and either the slope change at the knee or a common spectral index above the knee. Figure 10 shows such models fitting the Tibet array [23] and other flux measurements. The knee rigidity for such models is about 200 TV. Figure 11 shows that both such models are consistent with our composition measurements.

7 Conclusions

With the measurements of muon track angles in extensive air showers it is possible to obtain an 'average mass' parameter Λ of the cosmic-ray chemical composition in the 10^{14}–10^{16} eV energy range with $\Lambda \approx \langle \ln A \rangle / \ln 56$. The bias of air-shower

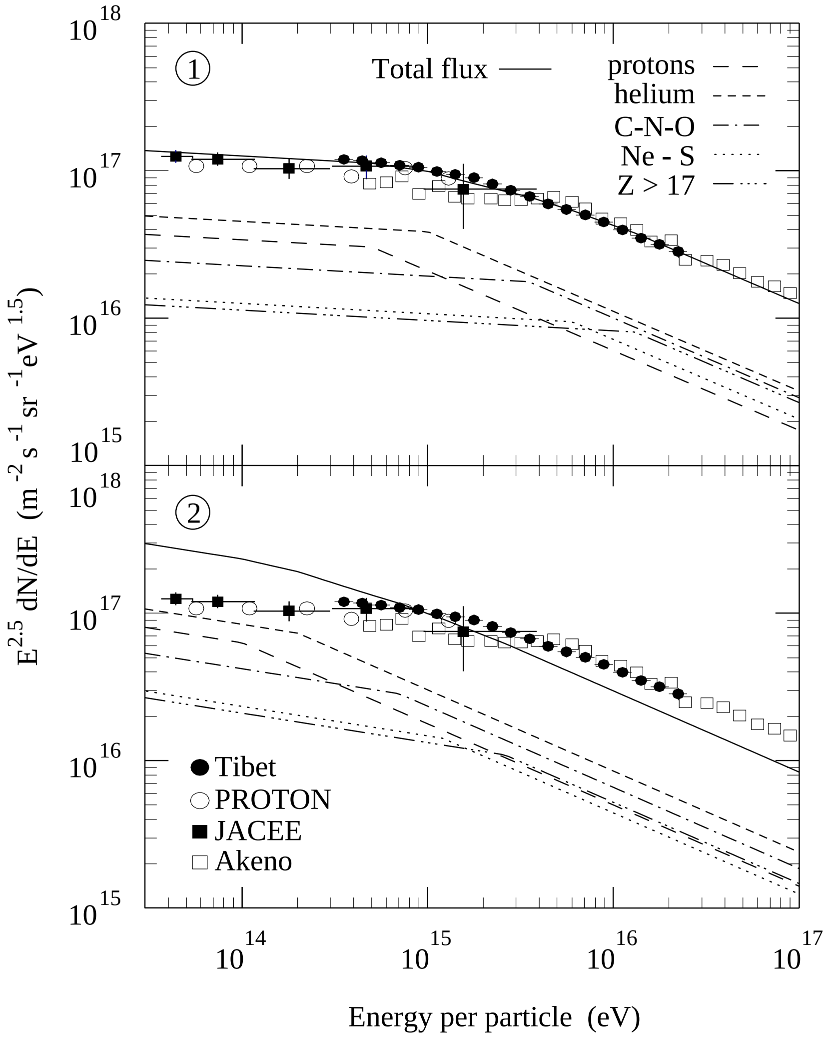

Figure 9: Fluxes scaled by energy $E^{2.5}$ of model compositions with a simple knee at fixed rigidity. Model 1: slope -2.57 below the knee rigidity of 500 TV and -3.04 above. Model 2: slope -2.7 below 100 TV and -3.05 above. Models are normalized to Tibet array measurements (for their HD1 model) [23] at 1 PeV. Also shown for comparison are flux measurements of the Proton [24], JACEE [17] and Akeno [22] experiments. Note that differences of the order of 30% between absolute flux scales by different experiments are consistent with their estimated energy scale errors.

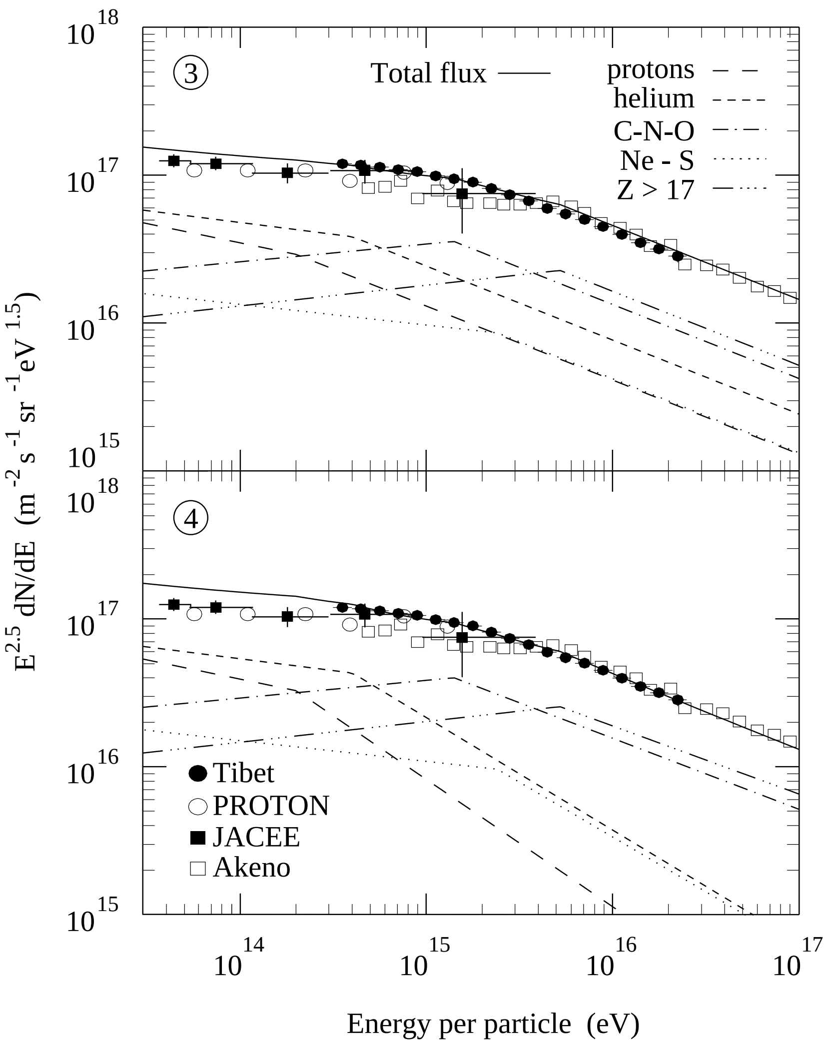

Figure 10: Fluxes of model compositions extrapolating JACEE measurements with an additional knee at a fixed rigidity of 200 TV. Model 3: slope changes to -3.01 above the knee. Model 4: slope steepens by 0.6 at the knee.

arrays in favour of showers induced by light primaries is cancelled to a very good approximation by the larger number of muons in showers of heavy nuclei.

The analysis of the median radial angles of muons in the CRT/HEGRA data set shows an increase of $\langle \ln A \rangle$ in the 10^{14}–10^{15} eV which agrees very well with the highest energy direct measurements made by the JACEE collaboration. A combined analysis of the CRT/HEGRA composition data and cosmic-ray flux data of several experiments shows that a *minimal* composition model with a simple knee at a fixed rigidity can only be matched to either the composition or the flux data but not simultaneously to both. Although it may be too early to conclude that the transition to a second type of Galactic cosmic-ray sources is seen, the composition of cosmic-rays from a possible second type of sources should be heavier than what is measured well below the knee but not made up entirely of heavy nuclei.

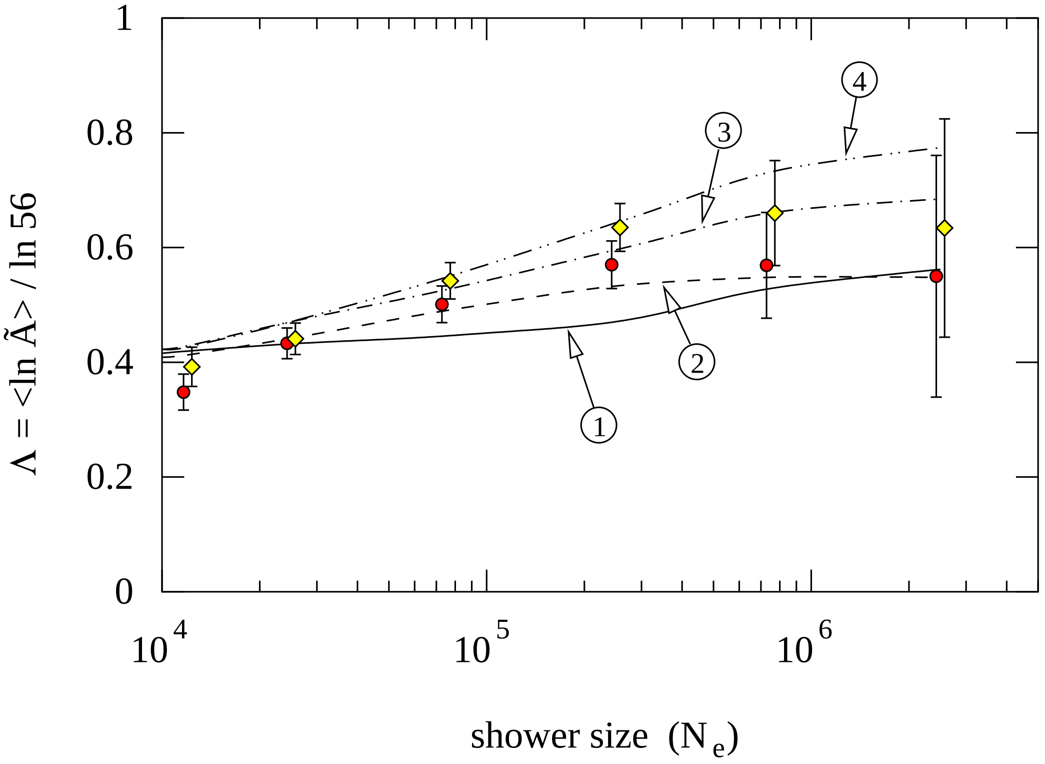

Figure 11: Values of Λ corresponding to composition models shown in figures 9 and 10 compared to CRT/HEGRA results for both choices of interaction models as in figure 8.

At the present level of accuracy of both composition and flux measurements an extrapolation of direct composition measurements with the additional constraint of a kink at a fixed rigidity of about 200 TV can describe the flux and composition measurements.

With the additional available data covering about half a year of combined CRT and HEGRA data taking (a four-fold of present statistics) the statistical errors even in our largest shower size interval would be well below present systematic uncertainties of the shower simulations. An extension to substantially larger shower sizes, however, would be difficult with the present installation because both CRTs and HEGRA would be affected by detector saturation.

Acknowledgements

We wish to thank the HEGRA collaboration very much for supporting the installation and operation of the CRT detectors at the HEGRA site and for providing the array data used in our analysis. It is a pleasure to thank also the authors of the CORSIKA shower simulation program, in particular J. Knapp and D. Heck. We thank the authorities of the Instituto de Astrofísica de Canarias (IAC) and the Roque de los Muchachos Observatory (ORM) for the excellent working conditions and for allowing measurements with CRT detectors outside of the HEGRA area. We gratefully acknowledge the technical support by the mechanical and electronic workshops of the MPIK.

References

[1] R. Blendford and D. Eichler, Phys. Rep. 154 (1987) 1.

[2] F. C. Jones and D. C. Ellison, Space Sci. Rev. 58 (1991) 259.

[3] B. A. Khrenov, in Cosmic Rays 92, ed. P. K. F. Grieder, pp. 18–33, Nuclear Physics B (Proc. Suppl.) 33 A,B, 1993.

[4] J. Wdowczyk, J. Physics G: Nucl. Part. Phys. 20 (1994) 1001.

[5] S. Petrera, Nuovo Cimento 19 C (1996) 737.

[6] K. Bernlöhr, Astroparticle Physics 5 (1996) 139.

[7] J. Heintze et al., Nucl. Instr. and Meth. A277 (1989) 29.

[8] K. Bernlöhr, Space. Sci. Rev. 75 (1996) 185.

[9] K. Bernlöhr et al., Nucl. Instr. and Meth. A369 (1996) 284.

[10] V. Fonseca, in Currents in High-Energy Astrophysics, ed. M. M. Shapiro, R. Silberberg, and J. P. Wefel, NATO ASI Series, Vol. 458, p. 143, Kluwer Academic Publishers, 1995.

[11] F. A. Aharonian and G. Heinzelmann, Proc. of the XVth European Cosmic Ray Symposium, Perpignan 1996, (in press).

[12] K. Bernlöhr et al., Nucl. Instr. and Meth. A369 (1996) 293.

[13] J. N. Capdevielle et al., The Karlsruhe Extensive Air Shower Simulation Code CORSIKA, Technical Report KfK 4998, Institut für Kernphysik, Forschungszentrum Karlsruhe, 1992.

[14] K. Werner, Phys. Rep. 232 (1993) 87.

[15] H. Fesefeldt, The simulation of hadronic showers, RWTH Aachen, Report PI-THA 85/02, 1985.

[16] K. Asakimori et al., Proc. 23rd Intern. Cosmic Ray Conf., Calgary, Vol. 2, pp. 21 and 25, 1993.

[17] K. Asakimori et al., 24th Intern. Cosmic Ray Conf., Rome, Vol. 2, p. 707 (e-print astro-ph/9509091) and T. Tominaga, private communication, 1995.

[18] Application Software Group, Computing and Networks Division, GEANT - Detector Description and Simulation Tool, CERN, Program Library Office, Geneva, Switzerland, 1993.

[19] H. Krawczynski, Diploma thesis, 1995.

[20] S. Martinez et al., Nucl. Instr. and Meth. A357 (1995) 567.

[21] H. Krawczynski et al., Nucl. Instr. and Meth. A 383 (1996) 431.

[22] M. Nagano et al., J. Physics G: Nucl Part. Phys. 10 (1984) 1295.

[23] M. Amenomori et al., Astrophys. J. 461 (1996) 408.

[24] N. L. Grigorov et al., Proc. 12^{th} Intern. Cosmic Ray Conf., Hobart, Vol. 5, p. 1746, 1971.